journal

J. Am. Ceram. Soc., 94 [S1] S112–S119 (2011)
DOI: 10.1111/j.1551-2916.2011.04496.x

Damage Evolution in Thermal Barrier Coatings with Thermal Cycling

Bauke Heeg

Lumium, Leeuwarden, The Netherlands

Vladimir K. Tolpygo

Honeywell Aerospace, Phoenix, Arizona 85034

David R. Clarke†

School of Engineering and Applied Sciences, Harvard University, Cambridge, Massachusetts 02138

Thermal barrier coatings typically fail on cooling after prolonged thermal cycling or isothermal exposure. The mechanics of spalling requires that first a critical sized portion of the coating separates from the underlying material, then buckles and finally spalls away. The critical size for buckling depends on the thickness of the coating but is several millimeters for typical zirconia coatings 150 μm thick. As-deposited coatings do not have interface separations but they form on thermal cycling as described in this work based on observations of coating cross-sections combined with the stress redistribution in the thermally grown oxide imaged using a piezospectroscopic luminescence method. Analysis of the images reveals that small, isolated regions of damage initially form and then grow, linking up and coalescing to form percolating structures across the coating until the buckling condition is attained, the buckle extends and failure occurs by spallation. The piezospectroscopic imaging of the stresses in the thermally grown oxide formed by oxidation beneath thermal barrier coatings provides a form of "stress tomography" enabling the subcritical separations to be monitored.

I. Introduction

One of the major themes of Tony Evans' research in the last decade, and one which we were privileged to collaborate with him, was the prime reliance of thermal barrier coating systems. Thermal barrier coatings have been in widespread use in commercial and military gas turbine engines for several decades providing thermal protection to superalloy components in the hottest sections of engines and in the last decade or so have been deemed "prime reliant." In some advanced engines, the coatings are in contact with gases that exceed the melting temperature of the superalloy blades and vanes.[1] In many respects, thermal barrier coatings must withstand the most demanding conditions that any ceramic component is subject to in today's technology but being ceramic materials, the coatings are prone to fail. The central scientific and engineering issue is to understand the failure mechanisms under different engine operating conditions and use that information to help identify conditions under which the coatings can be considered prime-reliant. This was the focus of an ONR Multi-University Research Initiative that Tony Evans led. The research described in this manuscript is a part of that quest.

Failure of TBCs is not well defined but is usually taken to have occurred when a portion of the coating has buckled and spalled away to expose a portion of the underlying component. Usually, this originates from edges but can also occur, especially on 1 in. diameter test samples, away from an edge. Irrespective of the origin, local buckling occurs before spallation as illustrated in the optical micrographs in Fig. 1. From images such as these and cross-sections of partially spalled coatings, failure occurs by an accumulation of damage until at some critical condition, yet poorly defined, the coating buckles, the buckle propagates and the coating then spalls away, leaving the underlying superalloy unprotected. The damage usually forms in the vicinity of the interface region between the thermal barrier coatings and the superalloy. Several mechanisms have been identified that can cause the onset of local damage but the mechanics of buckling[2–4] requires that a tensile stress perpendicular to the interface is necessary to form local separations or delaminations. In this contribution, we describe and quantify observations of the subcritical damage evolution obtained using microstructural observations made of polished cross-sections and by a nondestructive imaging method based on photo-stimulated luminescence piezospectroscopy (PSLS). The latter reveals the spatial distribution of the mean stress in the thermally grown oxide that forms between the thermal barrier oxide and the bond-coat. This, in turn, is sensitive to the extent of local damage in and around the TGO, including the TBC itself.

II. Materials

The 7 wt% yttria-stabilized zirconia (YSZ) coatings investigated in this work were deposited by electron beam evaporation onto flat platinum-modified nickel aluminide coated René N5 superalloy coupons by Howmet Research Center. The coatings were all similar to other state-of-the-art coatings made the same way but they were distinguished by all being from the same large batch of coatings deposited on 25 mm diameter, 3 mm thick superalloy disks all wafered from the same single crystal casting.

All the coatings were subjected to thermal cycling between room temperature and 1150°C with 1 h holds at the high temperature as has been described previously.[5] A sufficiently large number of coatings were tested that the average life of the coating batch under these thermal cycling conditions was established. This was determined to be 185 cycles. Some of the coatings were cycled to intermediate fractions of life rather than to spallation failure. Most of these were sectioned to characterize the damage at different fractions of life while four were subject to further analysis by PSLS[6] described in this work. The thermal diffusivities of these same coatings were also evaluated using a novel test based on the time delay in luminescence.[7]

A. Heuer—contributing editor

Manuscript No. 28809. Received October 21, 2010; approved February 11, 2011.
Part of the experimental work was conducted while at MetroLaser Inc., Irvine, CA.
†Author to whom correspondence should be addressed. e-mail: clarke@seas.harvard.edu

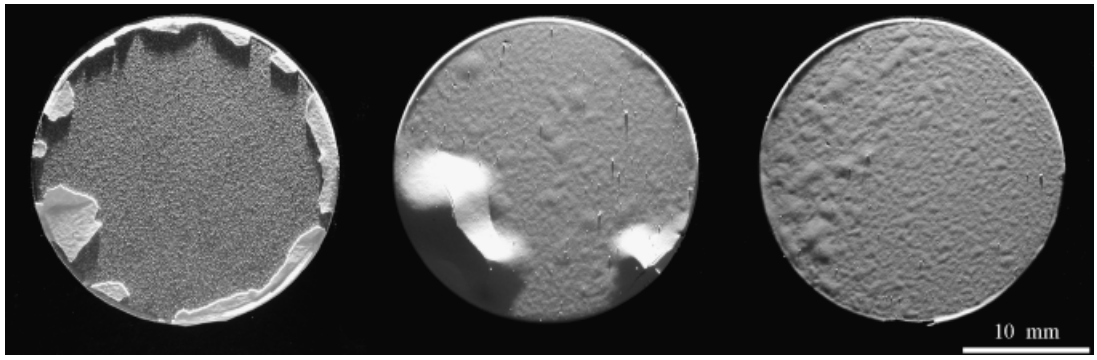

Fig. 1. Optical micrographs of EB-PVD deposited TBCs illustrating different stages in failure. Before macroscopic buckling (right), the formation of a macroscopic buckle (center) and after the TBC has everywhere spalled away except around the edges (left). The coated superalloy buttons are 25.4 mm (1 in.) in diameter.

III. Luminescence Imaging Modality

Microstructural examination of both cross-sections and fracture surfaces of thermal barrier coatings reveal that several types of local damage can be produced by thermal cycling. Figure 2, which is a composite of cross-sections recorded after deposition and after 25, 100, and 180 cycles, illustrates several of these damage types. In some cases, local separation or delamination occurs between the YSZ coating and the thermally grown oxide, such as at locations A. In other cases, local separation can occur between the thermally grown oxide and the metal although the majority of these separations may be caused by the cutting the cross-sections and subsequent polishing.

In still other cases, cracking takes place in the thermally grown oxide, such as at location B in Fig. 2(c). This occurs mainly where the TGO is locally deformed in bending. In the majority of cases, as well as in under isothermal testing, separation occurs within the YSZ coating in the vicinity of its interface with the thermally grown oxide. An example is seen at location C in Fig. 2(b). All of these separations are well below the outer surface of the coating and so none of these can be discerned through the coating itself under normal imaging conditions since the coatings are optically turbid because of scattering from internal pores. (It is possible to image some of these damaged regions with rather poor spatial resolution by mid-infra-red imaging at 3–6 μm where the scattering is weakest, as has been shown at NASA.[8] For thinner TBC, it is also possible to see separations in light microscopy.[9]) The depth beneath the coating surface over which the damage forms and localizes is also relatively narrow, substantially smaller than the coating thickness, and so cannot currently be resolved by X-ray tomography. While useful for visualization of the damage, direct imaging is nevertheless expected to be of limited value since it only provides areal information and no information about the local

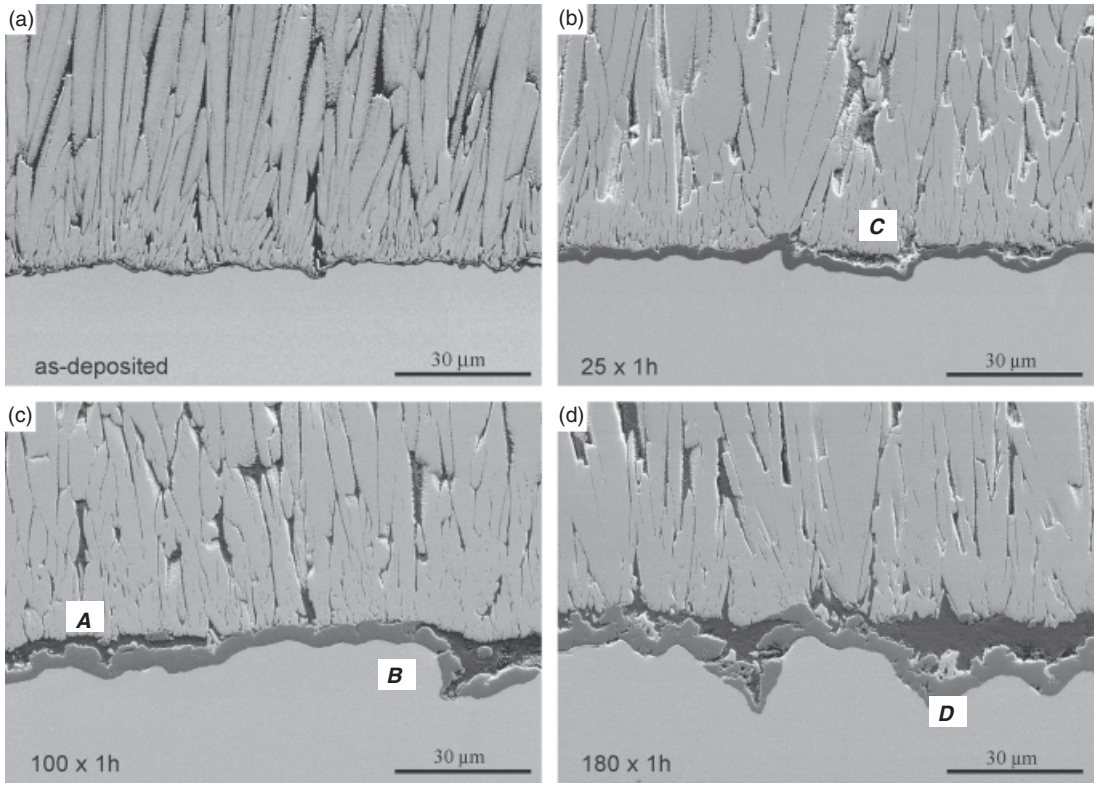

Fig. 2. Cross-sections of the alloy/TGO/TBC interfacial regions. (a) after deposition, and after (b) 25 (c) 100, and (d) 180 thermal cycles, each 1 h long, illustrating the thickening of the thermally grown oxide (TGO), the roughening of the interfaces, interface separations and the cracking of the TGO associated with the roughening. The TGO, which appears dark gray, is located between the columnar thermal barrier top-coat, above, and the aluminide bond-coated superalloy, below the TGO.

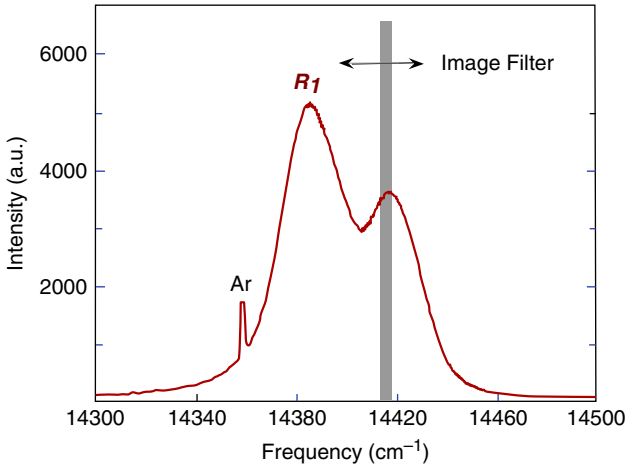

Fig. 3. Characteristic R-line luminescence from a TGO. The sharp line labeled Ar is from an argon discharge lamp used to calibrate frequency.

stresses or elastic strain energy that motivate failure. To provide this information, we have developed an imaging system for measuring the spatial distribution of the local strains in the TGO, by PSLS through the TBC.[6] In essence, the method uses the TGO as a strain sensor of the damage in its vicinity to monitor the stress re-distribution on thermal cycling.

(1) Piezospectroscopy

The physical basis of the piezospectroscopy technique has been described in detail previously so is only briefly summarized here.[10–14] The thermally grown oxide is aluminum oxide and contains trace concentrations of Cr^{3+} incorporated during its growth at high temperature. The Cr^{3+} ions luminesce when excited optically, producing a very sharp emission doublet at 694 nm, the R_1 and R_2 lines as illustrated in Fig. 3. The radiative and nonradiative transitions following the excitation of electrons from the ground state are shown in Fig. 4 with the R-lines resulting from emission from the split E2 state. Because the energy of the $2E \rightarrow 4A_2$ transition responsible for the R-line emission is sensitive to the overlap of the $3d^3$ orbitals, and consequently the distance between the Cr^{3+} ions and the surrounding O^{2-} ions, the wavelength of the R lines is sensitive to strain.[15] Measurement of the wavelength can thus be used to nondestructively monitor strain.[11] Although the stress dependence of the shift of the R_1 and R_2 lines is slightly different and is also dependent on both the crystallographic orientation of the alumina[11] as well as on polarization,[12,16] the frequency shift reduces to being proportional to the trace of the stress tensor, and hence the mean stress, σ_m

$$\bar{\Delta\nu} = \frac{\Pi_{ii}}{3}\langle(\sigma_{11} + \sigma_{22} + \sigma_{33})\rangle = \Pi_{ii}\sigma_m \qquad (1)$$

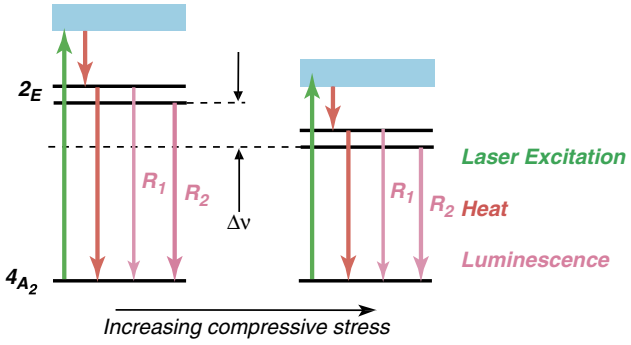

Fig. 4. Schematic of the energy levels of Cr^{3+} in alumina, the decay paths and the energy shift caused by a compressive stress.

for a polycrystalline alumina having a grain size that is much smaller than the probe size and where the grains are randomly oriented.[11,17] The trace of the piezospectroscopic coefficient tensor, Π_{ii}, has a value of 7.61 $(cm \cdot GPa)^{-1}$ for the R_2 line so by inverting Eq. (1), the mean stress can be obtained from the measured change in frequency from its' stress-free value. The intensity of the R-line luminescence is not dependent on stress and so variations in intensity due to, for instance, variations in TBC thickness, local optical scattering lengths or incident illumination, do not affect the value of the measured stress.

(2) Imaging System

Until recently, the stress distribution in the TGO could only be monitored point by point moving a focused laser beam across a coating and subsequently forming maps pixel by pixel, a laborious process ill-suited to evaluation of coatings on thermal cycling. In the imaging system shown schematically in Fig. 5, an area of interest on a coating is illuminated by a uniform laser beam and the luminescence is collected by a CCD camera, after filtering through a wavelength-tunable filter. A series of images, each at a slightly different narrow wavelength band, is recorded, thus mapping the R_1 and R_2 spectra for each pixel on the CCD. From this a map of the strain distribution is assembled by analyzing the spectra by software. Details of the algorithm for curve fitting and extracting the strain are described elsewhere.[18,19] The tunable filter is a motorized Fabry–Perot filter that only passes a very narrow band of the luminescence as illustrated schematically in Fig. 3. The observations described in this contribution were formed using a 1 W frequency doubled Nd:YAG laser (532 nm) and a low noise CCD camera (Santa Barbara Imaging Group, Goleta, CA). The mean stress is taken to be over the volume of the resolution element, i.e., the volume of the TGO corresponding to the measurement over an area projected onto a pixel of the CCD.

IV. Observations and Analysis

Images of the spatial distribution of the mean stress in four different coatings at the different fractions of thermal cycles are reproduced in Fig. 6. The values of the stresses are color coded (note that the stress-scale is adjusted in each case to optimize the color contrast). Each data point in the stress image corresponds to approximately 16 μm spatial resolution, such that the total imaged area is about 4.4 by 5.6 mm. Most measurements allow determination of the stress, except in a few locations where either luminescence is too weak or too strong. These areas are colored white. Apart from the evident variations in color there are no obvious spatial correlations in the stress variations that might indicate the size or extent of damage or its evolution. Analysis of the frequency distribution of the stresses extracted

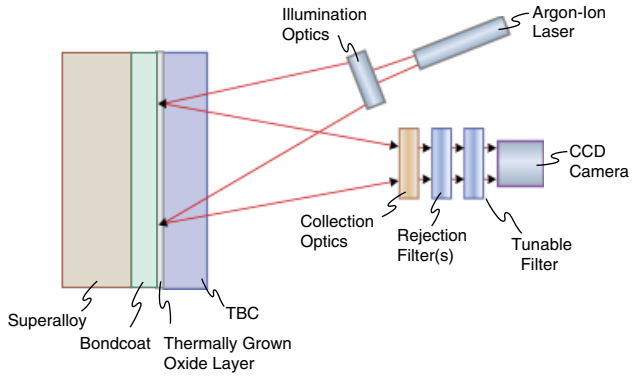

Fig. 5. Schematic of multispectral imaging system in which a TBC-coated sample is uniformly illuminated with an argon ion laser beam and the luminescence imaged onto a CCD through a variable wavelength tunable Fabry–Perot filter.

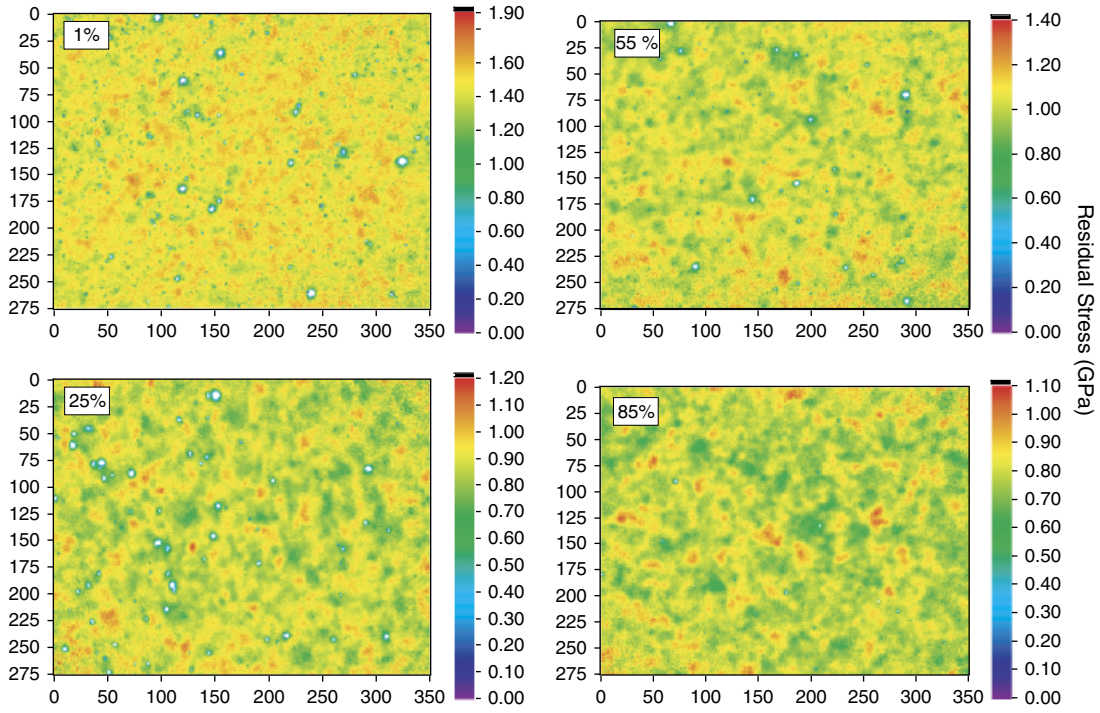

Fig. 6. Piezospectroscopic images of four coatings at different fractions of their average life. The color coding corresponds to the mean stress levels shown on the vertical color stripes on the right hand side of each panel. The numbers on the left hand ordinate and horizontal are pixels, each 16 μm in size, so the images correspond to areas of 4.4 mm × 5.6 mm.

from the images shown in Fig. 6 is more revealing. This data, Fig. 7, indicates that the average value of the mean stress decreases with thermal cycling, consistent with the release of elastic strain energy density. Furthermore, the stress variation over the imaged area more closely fits a Gaussian rather than a Weibull distribution, although this data is for the overall stresses rather than those in the immediate vicinity of the damaged regions. A Gaussian distribution indicates that stress values across the image can be interpreted as independent or at least of short lateral order, i.e., with little correlation between different subregions. This lack of correlation is also evident from an overall featureless two-dimensional Fourier transform (not shown).

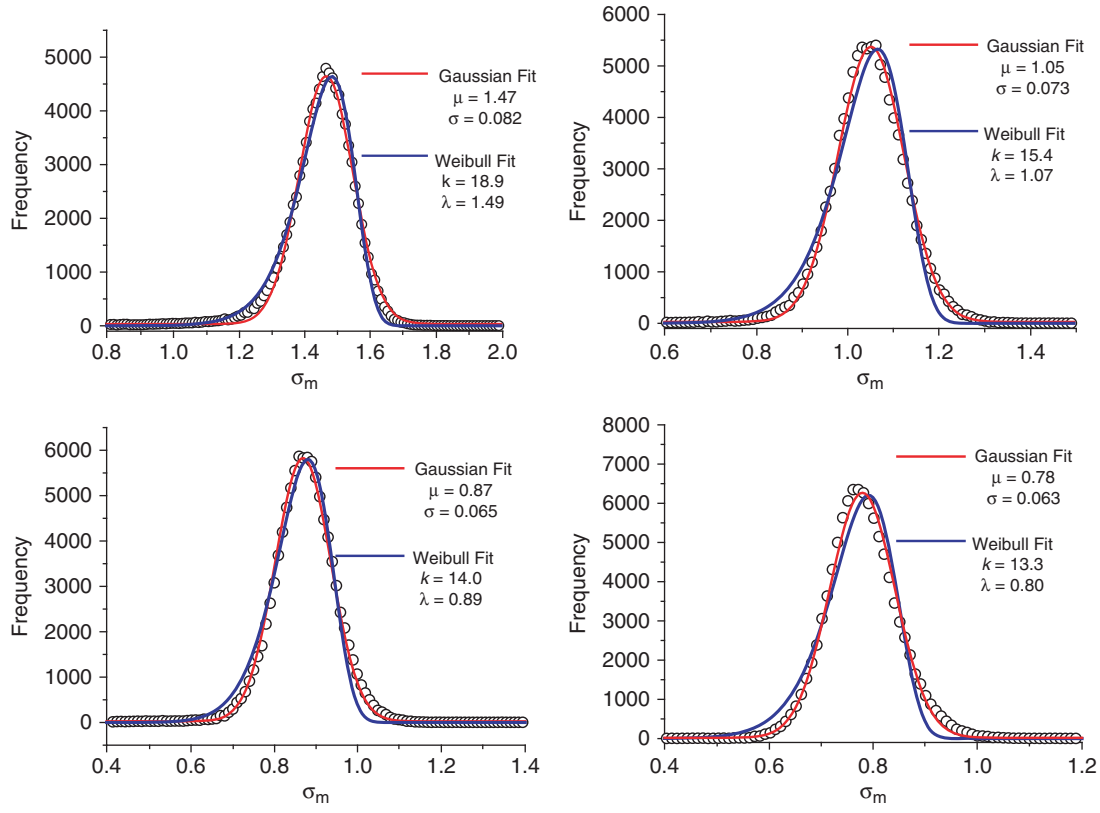

Fig. 7. Distribution functions of the stresses in the images shown in Fig. 6 as a function of the mean stress.

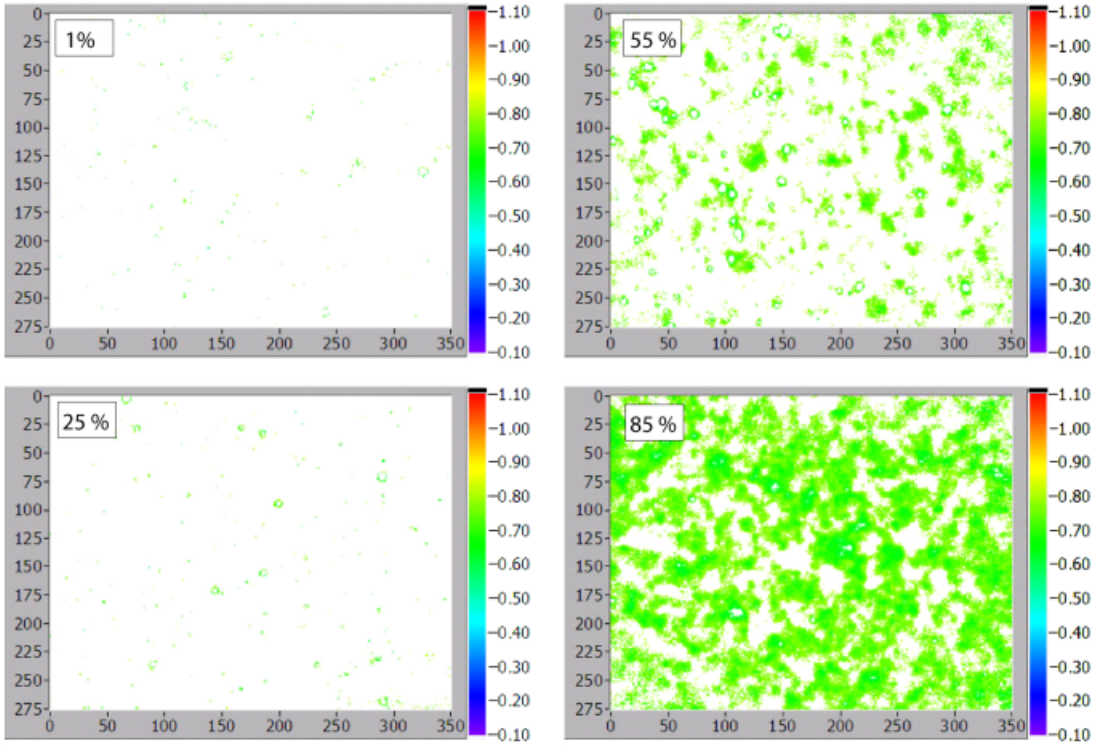

Fig. 8. Filtered piezospectroscopic images of Fig. 6 showing in green those regions where the mean stress in the thermally grown oxide is between 0.6 and 0.8 GPa. The white regions correspond to regions where the local mean stress is above 0.8 GPa. The numbers on the left hand ordinate and horizontal are pixels, each 16 μm in size.

Spatial correlations in the stress variation at particular stress intervals are more revealing. For instance, Fig. 8 are images formed by mapping out those regions of the four samples where the stresses lie between 0.6 and 0.8 GPa, an arbitrary stress interval. As can be expected from the stress distribution functions shown in Fig. 7, only small regions of the coatings at early stages of life are below this threshold. By 55% of life, 15.5% of the area lies within this stress interval and by 85% of life, about 60% of the area. While these numbers provide an additional quantification not obvious in the stress images, the image at 85% life suggests a new insight, namely that percolation of the damage appears to occur toward the end of life. Another way of representing the same data is by plotting the fractional area within this stress interval as a function of the life as in Fig. 9. This suggests that the fractional area grows as a power law function of the number of thermal cycles.

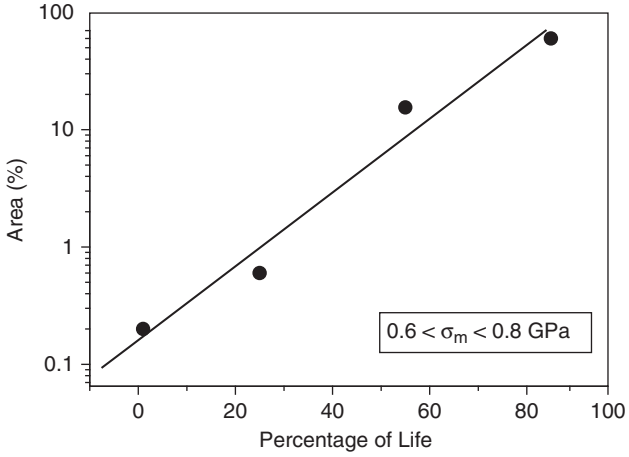

Fig. 9. Fractional area of the coatings where the mean stress lies in the interval 0.6–0.8 GPa as a function of the fractional life. Data obtained from the piezospectroscopic images in Fig. 6.

To quantify the size and number of local separations, cross-sections of the coatings were analyzed. In each case, the number and length of the individual separations along the coating interface were measured and recorded. From this quantification procedure, carried out on coatings exposed for a number of different thermal cycles, a number of variables were analyzed: proportion of the interface that was separated, interface roughness, the average length of the separations, and the size of the largest separation. In addition, the luminescence shift was recorded through the TBC before cross-sectioning. The results of these analyzes are summarized in Fig. 10. Figure 10(a) shows that the number of separations per unit length of interface at first increases, reaches a maximum and then decreases with the number of cycles until, at failure, it approaches one. Before cycling begins, a small number of separations are already present, seemingly randomly distributed along the interface. The initial increase indicates that new separations form, and after reaching a maximum, the number decreases as individual separations coalesce at a greater rate than fresh separations nucleate. No unique function describes the data but its functional form is similar to that of nucleation and growth in two-dimensions. Complementary is the data in Fig. 10(b) of the proportion of the interface that is separated as a function of the number of cycles. This is a monotonic function that asymptotes to unity as failure is approached. The piezospectroscopic shift decreases monotonically with thermal cycle life as shown in Fig. 10(c). Data from both the measurements as well as the PS imaging analysis results are shown. The last set of data obtained from analysis of the cross-section images is the lateral size of the separations shown in Fig. 10(d). Interestingly, both the average separation size and the size of the largest separation increase as a power-law function of the number of thermal cycles. This data suggests that separations do grow by coalescence. Furthermore, although there is greater statistical variation and fewer measurements could be made, the size of the largest separation increases at a faster rate than does the average size. The

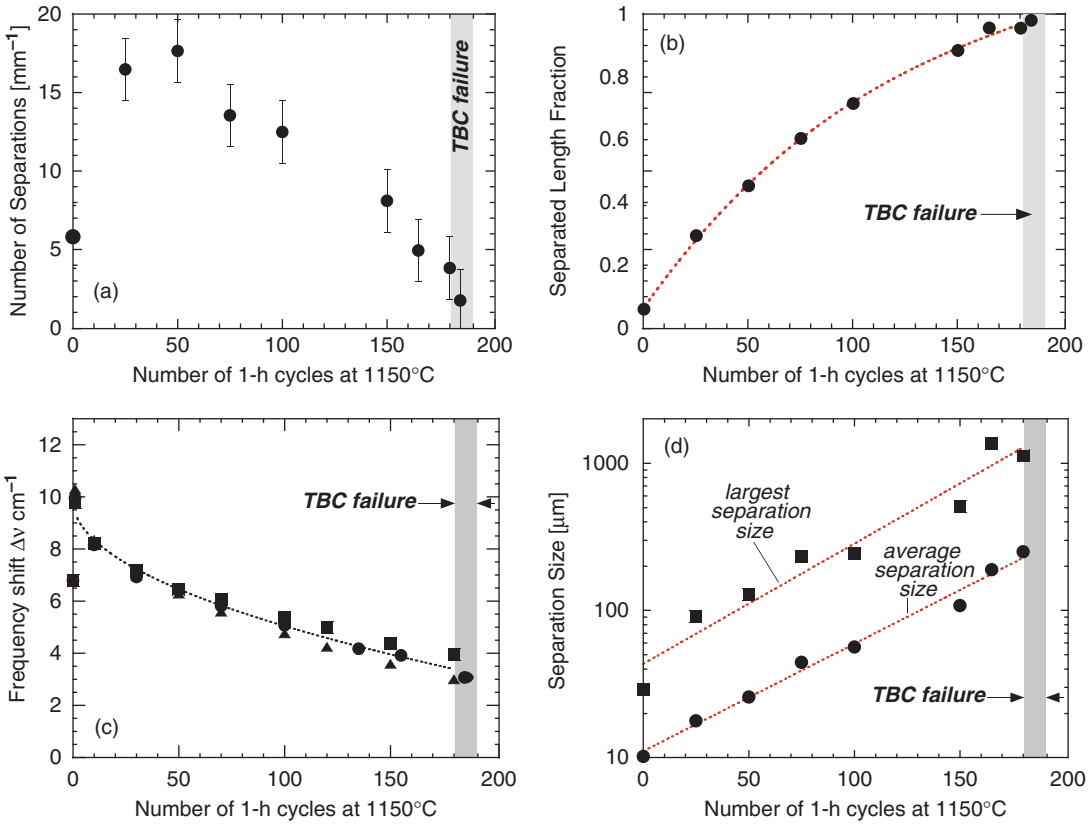

Fig. 10. Data obtained from analysis of SEM cross-sections. (a) Number density of separations, (b) proportion of the interface length that has separated, (c) piezospectroscopic shift, and (d) lateral size of interface separations, all as a function of the number of thermal cycles.

implication is that the largest separation grows by linking up larger separations.

V. Discussion

The cross-sectional microstructural analysis and the piezospectroscopy images provide complementary information concerning the damage evolution with thermal cycling. Comparison of the results also provides confidence in the interpretation of the piezospectroscopy images. Together, these results clearly, and unambiguously, show that well before macroscopic buckling and spallation occurs, the EB-PVD coatings on Pt-modified aluminized superalloy coupons begin to fail by a sequence of events in which local separations nucleate in the vicinity of the TGO, grow and link up. In this and several previous studies by different groups,[20–22] it has been found that the mean stress in the TGO is highest immediately after deposition of the TBC, when the alloy surface is flattest, and then monotonically decreases with thermal cycling as illustrated in Fig. 10(d). The large, mean compressive stress is attributed to the thermal expansion mismatch between the initially flat TGO and the underlying alloy as well as a compressive growth stress in the TGO. With thermal cycling the compressive stress decreases. This is a result of damage to the TGO, such as shown in Fig. 2, and change in shape as the TGO deforms to conform to the shape of the evolving bond-coat surface and constrained by the TBC on top of it. The change in shape causes the initial approximately biaxial stress state in the TGO to become increasingly tri-axial with out-of-plane tensile and compressive stresses. (The stress state is only approximately biaxial because the alloy is not entirely flat but has some initial roughness.) Insufficient data yet exists to determine the most appropriate physically based mathematical description of the decrease in mean stress but it can be fit to a form

$$\sigma_m = a - b\,t^n \tag{2}$$

where a and b are constants and the exponent n is approximately 0.5. As the strain energy density in the TGO is proportional to the square of the mean stress, this would imply that the overall driving force in the TGO for further damage is also decreasing with thermal cycling. However, as will be described later in this section, the crack driving force for TBC failure is likely to be more complicated since there is strain energy in the TBC as well as in the TGO.

Analysis of the cross-section images indicates that local separations can exist even before thermal cycling begins. Whether these are the result of local contamination, the thermal stresses associated with cooling from deposition or shadowing during deposition is not known but it is evident that during the early stages of thermal cycling, other separations form along the interface. At the same time, as evident in both the PSLS images and the cross-sectional images, these local separations grow and begin to link up and coalesce to form clusters of local damage. Throughout the life, the average size of the separated regions, as well as their largest size, C_L, increase with the number of thermal cycles as a power law function

$$C_L = C_0\,N^n \tag{3}$$

where C_0 is an initial size. Furthermore, although the average value of the mean stress decreases with the number of thermal cycles as mentioned above, the probability distribution in stress across the coatings appears to remain Gaussian. However, further analysis of the "low stress" portion of the stress distributions is needed to ascertain more about how the actual statistics of the coalescence process.

The current study does not provide any new insights into the origin of the local interface separations but it is assumed that separations form in response to the development of out-of-plane tensile stresses. This is consistent with an inability of the TGO and TBC to conform, by creep or plasticity, to the displacements

of the bond-coat surface produced by a combination of rumpling and swelling that occur with thermal cycling. Rumpling causes local bending of the TGO, creating out-of-plane strains and stresses, which not only decrease the mean stress in the TGO but also can produce TGO cracks by local tension or tearing. An example of this form of cracking is shown at B in Fig. 2. Inhomogeneous swelling, in particular, of the bond-coat from preferential nickel diffusion into the bond-coat from the underlying superalloy will cause nonuniform spatial displacements of the surface, promoting rumpling. This is believed to be responsible for separations of the type shown at D in Fig. 2. If the TBC is thick enough and remains in contact with the TGO, it suppresses rumpling. However, preexisting separations at the TBC/TGO interface or local regions where there are gaps in the TBC columns, either as a result of shadowing or very small grains, would result in less constraint and allow local rumpling and hence the development of out-of-plane tensile stresses. In some cases, as at location D in Fig. 2(d), the local TBC constraint is lost as a divot of TBC, a small wedge shaped grain formed at the intersection of two larger misoriented columns, appears to have been pulled away by the differential bond-coat motion.

Our finding that TBCs fail by a progressive nucleation, growth and linkage process until linked damaged regions extend across an area corresponding to the macroscopic buckling condition, provide some insight into why the thermal cycle life is sensitive to so many thermal cycling conditions.[5,23] Long hot times combined with slow heating and cooling rates and relatively low maximum temperature leave the bond-coat surface relatively flat and unchanged roughness and so the stresses normal to the interfaces are small and few local separations can occur. The lives are consequently relatively long. Under these conditions, it is speculated that processes that lower the interface fracture toughness cause failure such as might occur by long-range diffusion of species, for instance, S, from the underlying superalloy. Under these conditions, failure tends to occur once a critical thickness of the TGO is formed by oxidation and separation occurs preferentially by delamination along the bond-coat/TGO interface. The life can then be reasonably well predicted by oxidation life codes, such as COATLIFE,[24,25] embodying a critical thickness based on attaining a critical strain energy in the TGO and TBC. At the other extreme is rapid, short cycling at high temperatures, above about 1100°C. The lives under these conditions do not fit the oxidation life codes as has been remarked by Chan *et al.*,[24] being both much shorter and having a much larger statistically variability. These conditions, more typically encountered in military engines, are known to produce pronounced rumpling of bare PtNiAl aluminide coatings and, as illustrated in this work, several different types of interface damage but few bond-coat/TGO delaminations. Experiments and models indicate that at temperatures of 1100°C and above, the surface displacements are dependent on not only temperature but heating and cooling rates in the thermal cycles, too.[5,23,26] Consequently, there remains an outstanding problem of how to relate thermal cycle life to both maximum temperature and thermal cycle time, reconciling Eqs. (2) and (3) introduced above.

The complexity of the damage observed makes it difficult to describe failure in terms of detailed crack driving forces and fracture resistances. Not only does the propagation of a single crack seem an inappropriate description for the failure until the latest stages of the failure but also the separations are not strictly coplanar. Furthermore, although the luminescence shift is a measure of the mean stress it does not provide any information about the thickness of the TGO and hence is not a direct measure of the elastic strain energy, U_{SE}. Neither does it explicitly include the strain energy in the TBC. Nevertheless, as fracture of the TGO does not decrease its elastic modulus, the stored elastic strain energy in the TGO is proportional to the square of the mean stress. The TGO thickens by oxidation and so its thickness increases approximately parabolically with time. Consequently, the total elastic strain energy will be a slowly varying function of time. As the fracture resistance is unlikely to change very rapidly with thermal cycling, the critical condition for fracture at which the total strain energy area density equals the fracture resistance is likely to be poorly defined and variable. Consequently, one might expect that the failure life exhibits a large statistical variation about a mean value determined by the thermal cycling conditions. Furthermore, as described by Hutchinson in a companion article, failure (as well as buckling) occurs under mixed mode conditions, so the statistical variability is expected to be even greater than just discussed. Further complicating any detailed energy balances is the fact that the TBC sinters with time increasing its elastic modulus and with its strain energy. This emphasizes the importance of knowing where the separations lie; if they lie largely above the TGO, it's the strain energy in the TBC that provides the driving force for failure, whereas if the separations are principally at the alloy/TGO interface, then the strain energy in both the TGO and TBC must be included.

Finally, the imaging system used in this work remains a prototype. Further improvements in the optics as well as image processing hardware and software, currently being developed, can be expected to yield faster imaging of the stresses and make it possible to follow the damage evolution in even greater detail. For instance, the instrumentation should enable images of the residual stresses to be generated after each thermal cycle of the same test object, so that the growth and coalescence of individual separation events can be followed with cycling. The ability to generate large databases of residual stress data also allows better estimates of variance in residual stress data between samples for a given fractional life, in comparison with the current results based on a few samples. With better knowledge of the conditions for delamination coalescence, the image system promises to provide nondestructive monitoring of the health of individual blades and vanes. This would also facilitate comparison of our laboratory scaling findings to those on engine hardware as well as other types of coatings, including overlay coatings.

Acknowledgments

The authors are grateful to Ken Murphy of Alcoa Howmet Research Center for providing the coatings studied in this work. The authors are also grateful for support from the Office of Naval Research (D. R. C., V. K. T.) and the Air Force Research Laboratory (B. H., while at MetroLaser).

References

[1]T. Editors, "Britain's Lonely High-Flier"; The Economist, 2009
[2]A. G. Evans and J. W. Hutchinson, "On the Mechanics of Delamination and Spalling in Compressed Films," *Int. J. Solids Struct.*, **2**, 455–66 (1984).
[3]M. D. Thouless, H. M. Jensen, and E. G. Liniger, "Delamination from Edge Flaws," *Proc. Roy. Soc.*, **A447**, 271–9 (1994).
[4]J. W. Hutchinson and Z. Suo, "Mixed Mode Cracking in Layered Materials," *Adv. Appl. Mech.*, **29**, 63–191 (1992).
[5]V. K. Tolpygo and D. R. Clarke, "Rumpling of CVD (Ni,Pt)Al Diffusion Coatings Under Intermediate Temperature Cycling," *Surf. Coat. Technol.*, **203**, 3278–85 (2009).
[6]R. J. Christensen, D. M. Lipkin, D. R. Clarke and K. Murphy, "Nondestructive Evaluation of the Oxidation Stresses Through Thermal Barrier Coatings Using Cr^{3+} Piezospectroscopy," *Appl. Phys. Lett.*, **69** [24] 3754–6 (1996).
[7]B. Heeg and D. R. Clarke, "Optical Measurement of the Thermal Diffusivity of Intact Thermal Barrier Coatings," *J. Appl. Phys.*, **104**, 113119, 7pp (2008).
[8]J. I. Eldridge, C. M. Spuckler, and R. E. Martin, "Monitoring Delamination Progression in Thermal Barrier Coatings by Mid-Infrared Reflectance Imaging," *Int. J. Appl. Ceram. Technol.*, **3** [2] 94–104 (2006).
[9]V. K. Tolpygo and D. R. Clarke, "Morphological Evolution of Thermal Barrier Coatings Induced by Cyclic Oxidation," *Surf. Coat. Technol.*, **163–164**, 81–6 (2003).
[10]Q. Ma and D. R. Clarke, "Stress Measurement in Single-Crystal and Polycrystalline Ceramics Using their Optical Fluorescence," *J. Am. Ceram. Soc.*, **76** [6] 1433–40 (1993).
[11]Q. Ma and D. R. Clarke, "Piezospectroscopic Determination of Residual-Stresses in Polycrystalline Alumina," *J. Am. Ceram.c Soc.*, **77** [2] 298–302 (1994).
[12]S. H. Margueron and D. R. Clarke, "The Use of Polarization in the Piezospectroscopic Determination of the Residual Stresses in Polycrystalline Alumina Films," *Acta Mater.*, **54** [20] 5551–7 (2006).
[13]B. Heeg and D. R. Clarke, "Non-Destructive Thermal Barrier Coating (TBC) Damage Assessment Using Laser-Induced Luminescence and Infrared Radiometry," *Surf. Coat. Technol.*, **200** [5–6] 1298–302 (2005).

[14]J. A. Nychka and D. R. Clarke, "Damage Quantification in TBCs by Photo-Stimulated Luminescence Spectroscopy," *Surf. Coat. Technol.*, **146**, 110–6 (2001).
[15]B. Henderson and G. F. Imbusch, *Optical Spectroscopy of Inorganic Solids*. Claredon Press, Oxford, 1989.
[16]D. J. Gardiner, M. Bowden, S. H. Margueron and D. R. Clarke, "Use of Polarization in Imaging the Residual Stresses in Polycrystalline Alumina Films," *Acta Mater.*, **55**, 3431–56 (2007).
[17]D. R. Clarke and D. J. Gardiner, "Recent Advances in Piezospectroscopy," *Int. J. Mater. Res.*, **98**, 1–8 (2007).
[18]B. Heeg and J.B Abbiss, "Piezospectroscopic Imaging with a Tunable Fabry-Perot Filter and Tikhonov Reconstruction," *Opt. Lett.*, **32** [7] 859–61 (2007).
[19]J. B. Abbiss and B. Heeg, "Imaging Piezospectroscopy," *Rev. Sci. Instrum.*, **79**, 123105, 9pp (2008).
[20]M. Wen, E. H. Jordan, and M. Gell, "Evolution of Photostimulated Luminescence of EB-PVD (Ni,Pt)Al Thermal Barrier Coatings," *Mater. Sci. Eng.*, **A398**, 99–107 (2005).
[21]V. K. Tolpygo, D. R. Clarke, and K. S. Murphy, "The Effect of Grit Blasting on the Oxidation Behavior of a Platinum-Modified Nickel-Aluminide Coating," *Metall. Mater. Trans. A-Phys. Metall. Mater. Sci.*, **32** [6] 1467–78 (2001).
[22]G. Lee, A. Atkinson, and A. Selcuk, "Development of Residual Stress and Damage in Thermal Barrier Coatings," *Surf. Coat. Technol.*, **201** [7] 3931–6 (2006).
[23]V. K. Tolpygo and D. R. Clarke, "Temperature and Cycle Time Dependence of Rumpling in Platinum-Modified Diffusion Aluminide Coatings," *Scri. Mater.*, **57**, 563–6 (2007).
[24]K. Chan, S. Cheruvu, and R. Viswanathan, "Development of a Thermal Barrier Coating Life Model"; pp. 591–5 in *ASME Turbo Expo 2003*. ASME, Atlanta, 2003.
[25]T.A Cruse, S. E. Stewart, and M. Ortiz, "Thermal Barrier Coating Life Prediction Model Development," *J. Eng. Gas Turbines Power*, **110**, 610–6 (1988).
[26]D. S. Balint and J. W. Hutchinson, "An Analytical Model of Rumpling in Thermal Barrier Coatings," *J. Mech. Phys. Solids*, **53** [4] 949–73 (2005). □